HIGH SURFACE AREA ZINC ELECTRODE FOR FURFURAL ELECTROCATALYTIC HYDROGENATION

By

Seungyeon Lee

A THESIS

Submitted to
Michigan State University
in partial fulfillment of the requirements
for the degree of

Chemical Engineering – Master of Science

2022

ABSTRACT

HIGH SURFACE AREA ZINC ELECTRODE FOR FURFURAL ELECTROCATALYTIC HYDROGENATION

By

Seungyeon Lee

With the increasing need to achieve carbon neutrality, electrocatalytic hydrogenation (ECH) of biomass-derived oxygenates, such as furfural, has received growing interest. Biomass ECH is an eco-friendly conversion of an abundant resource to valuable chemical products like fuels that replace fossil resources. In this study, we focus on high surface-area zinc nanoparticles as a catalyst for furfural ECH. The rotating disk electrode (RDE) is employed to enable quick electrochemical studies with small surface area, and kinetic parameters were obtained via Koutecký-Levich analysis. To modify a glassy carbon RDE with zinc nanoparticles, Nafion®, polyvinyl pyrrolidone (PVP), and polyvinyl alcohol (PVA) were studied as binders.

In the absence of furfural, chronoamperometry of PVA-bound zinc electrodes showed continuous steady current associated with the hydrogen evolution reaction (HER). In contrast, Nafion® and PVP bound electrodes were found to be unstable. In the presence of furfural, high electrocatalytic activity was achieved with Zn-PVA compared to glassy carbon. The Zn-PVA electrode was optimized by varying the binder content and total zinc loading. A weak optimum was identified at 92 wt% zinc and 8.6 mg_{Zn}/cm^2 loading. For zinc electrodes, high FE was obtained at higher overpotential (-0.9V vs. RHE), whereas higher FE was obtained at lower overpotentials for copper. Through Koutecký-Levich analysis, kinetic current densities and moderate Tafel slopes were observed, suggesting that the high surface-area zinc electrode is a promising platform for ECH. Product analysis studies using GC-MS are suggested to verify FE and to further elucidate the mechanism of furfural ECH at zinc electrodes.

Dedicated to Dad, Mom and Sonya

ACKNOWLEDGEMENTS

I would like to express my sincere gratitude to my advisor, Dr. Scott Calabrese Barton, for his guidance and support throughout my graduate program. His advice carried me to become a better researcher with patience and passion. I would not have made this far if it was not for Dr. Barton. It has been an honor and a privilege to have worked with an amazing professor and a mentor.

I thank my committee members, Dr. David Hickey and Dr. Robert Ofoli. I am glad that I was able to continue working with Dr. Hickey for my Master's program, after my senior year at Michigan State working as a grader for CHE 210 for his class. I am also happy to have the opportunity to work with Dr. Ofoli because you have been an inspiration to all of Chemical engineering students in CHE 301 and CHE 312.

I would also like to acknowledge Dr. Maddalena Fanelli who have encouraged me to apply for Engineering Summer Undergraduate Research Experience (*EnSURE*) program. She is one of the best chemical engineering professors I know at MSU who always cares for students to succeed. From *EnSURE*, I have met amazing group of people in Dr. Roozbeh Dargazany's High-Performance Materials group. I want to express my gratitude to Dr. Dargazany, Mamoon, Yang, Sharif, Wanru, and Abdo.

I also thank Dr. Timothy Hinds, Dr. Christina Chan, Dr. Richard Lunt, Dr. K Jayaraman, Dr. Gary Blanchard, Dr. Virginia Cangelosi, Dr. Amy Pollock, Dr. Brittany Busby, and Johanna Herman for providing me opportunity to mentor and interact with STEM major students as a *Cornerstone & Residential Experience Engineering* tutor, a grader in CHE 210 and CHE 311, and a graduate teaching assistant in CEM 141 and CEM 162 throughout my journey at MSU. I

would like to thank Dr. Carl Lira and Dr. Lars Peereboom for providing me access and helping me get trained to gas chromatography.

I would like to thank my groupmates as well. My mentor and a collaborator, Manali, was my former TA in CHE 431. She is such a brilliant chemical engineer and also a good mentor who had helped me a lot in lab. I could not have done this far without her. I thank Alex, Brandon, Christina, Jim, Samin, Yan, and Yunlu for also being supportive and encouraging me. I have really blessed to build such an amazing friendship with all these wonderful, kind, and smart people.

I thank all my best friends at MSU. Alex and I would always work on projects every day and I miss those days sometimes when I walk in EB. Alex is such an amazing, smart friend and a great team player. Matt and I have known since my freshman year in CEM 161. I am so blessed to have met such a kind, supportive friend who would always care for me. Mariah is the sweetest person and my best friend for life. Although we have spent most of our time together in EB or MSU main library, her positivity is what made me feel alive and happy. I would never trade my friendship with Alex, Matt, and Mariah for anything. Their effort trying to spell my Korean name makes me feel special. I hope that we can all meet together one time in Korea. I also thank Erin for being my best roommate in college. I thank my friends from Phi Sigma Rho, Blaire, Ava, and Allyson, and my friends from high school, Ayeon, Hyojin, Yehji, and Jongwon.

Last but not least, I cannot thank my family enough who have supported me no matter what. My dad, mom, and my sister have always encouraged me, and helped me get through COVID by facetiming every night and playing games together. I cannot wait to see you all! I love you so much and thank you for loving me unconditionally.

TABLE OF CONTENTS

LIST OF TABLES

LIST OF FIGURES

KEY TO SYMBOLS AND ABBREVIATIONS

A	Electrode surface area (cm^2)
α_α	Anodic transfer coefficient
α_c	Cathodic transfer coefficient
C	Concentration of furfural (mol)
D	Diffusion coefficient (m^2/s)
F	Faraday's constant (96,485 C mol^{-1})
i	Current density (mA/cm^2)
i_{cd}	Current density (mA/cm^2)
i_d	Limiting current density (mA/cm^2)
i_k	Kinetic current density (mA/cm^2)
i_o	Exchange current density (mA/cm^2)
R	Gas constant (8.314 J/mol K)
T	Temperature
n	Number of electrons transferred
η_s	Surface overpotential (V)
ω	Rotating speed of electrode (rpm)
W_f	Swollen weight of polymer (g)
W_i	Initial dried weight of polymer (g)
V	Working electrode potential
v	Kinematic viscosity of solution (m^2/s)

BET	Brunauer-Emmett-Teller
CA	Chronoamperometry
CE	Counter electrode
CV	Cyclic voltammetry
DIW	Deionized water
ECH	Electrocatalytic hydrogenation
EDX	Energy dispersive x-ray
EG	Ethylene glycol
EtOH	Ethanol
FA	Furfuryl alcohol
FE	Faradaic efficiency
GA	Glutaraldehyde
HER	Hydrogen evolution reaction
IPA	Isopropyl alcohol
LSV	Linear sweep voltammatery
MF	2-methylfuran
MTHF	Methyl tetrahydrofuran
NP	Nanoparticle
ORR	Oxygen reduction reaction
PVA	Polyvinyl alcohol
PVP	Polyvinyl pyrrolidone
RDE	Rotating disk electrode
RE	Reference electrode

RHE	Reversible hydrogen electrode
SEM	Scanning electron microscopy
THF	Tetrahydrofuran
THFA	Tetrahydrofurfuryl alcohol
WD	Working distance

1. Introduction

Due to rapid climate change caused by the mass use of fossil fuels, it has become a universal goal to tackle global warming through reducing CO_2 emissions. During the COVID-19 pandemic lockdown, there was a 5.4% drop in carbon emissions from fossil fuels.[1] However, in several countries where lockdown was not mandatory, carbon emissions increased during pandemic.[2] Similarly, BP (British Petroleum) has reported that energy consumption increased gradually over time, except for a 4.5% decrease during pandemic.[3] Therefore, it can be interpreted that our human activities have a significant impact on climate change. It also stresses the importance of discovering strategies to lessen the greenhouse effect.

Another motivation for replacing fossil fuels is due to their scarcity. Renewable energy is an excellent replacement because it can be replenished and help reduce the reliance on non-renewable energy source. Biomass is one of the abundant energy sources, that is derive from plants and animal wastes.[4] There are two main groups of biomass that produce bio-oils; lignocellulose are forest- or crop-based while triglycerides are based on agricultural fats and oils.[5] Lignocellulose can be classified into cellulose, hemicellulose, and lignin.[5] Cellulose is a linear polymer with a general formula of $(C_6H_{10}O_5)_n$ composed of D-glucose subunits connected with β-1,4 glycosidic bonds.[6,7] Hemicellulose has a general formula of $(C_5H_8O_4)_n$ composed of sugars such as L-arabinose, D-glucose, D-mannose, D-xylose, D-galactose, etc. that are connected with β-1,3 or β-1,4 glycosidic bonds, making it a complex polymer structure.[6] Lignin is an amorphous heterogeneous polymer composed of phenylpropane units.[6] Triglycerides are composed of three fatty acids per one glycerol molecule.[5]

Xylose is one of the most abundant hemicellulose derived compounds with five carbon atoms.[8] An acid catalyzed dehydration of xylose produces furfural, a furanic compound that has

a ring structure with one oxygen atom.[9–11] The chemical structure of furfural can be seen in Figure 1.

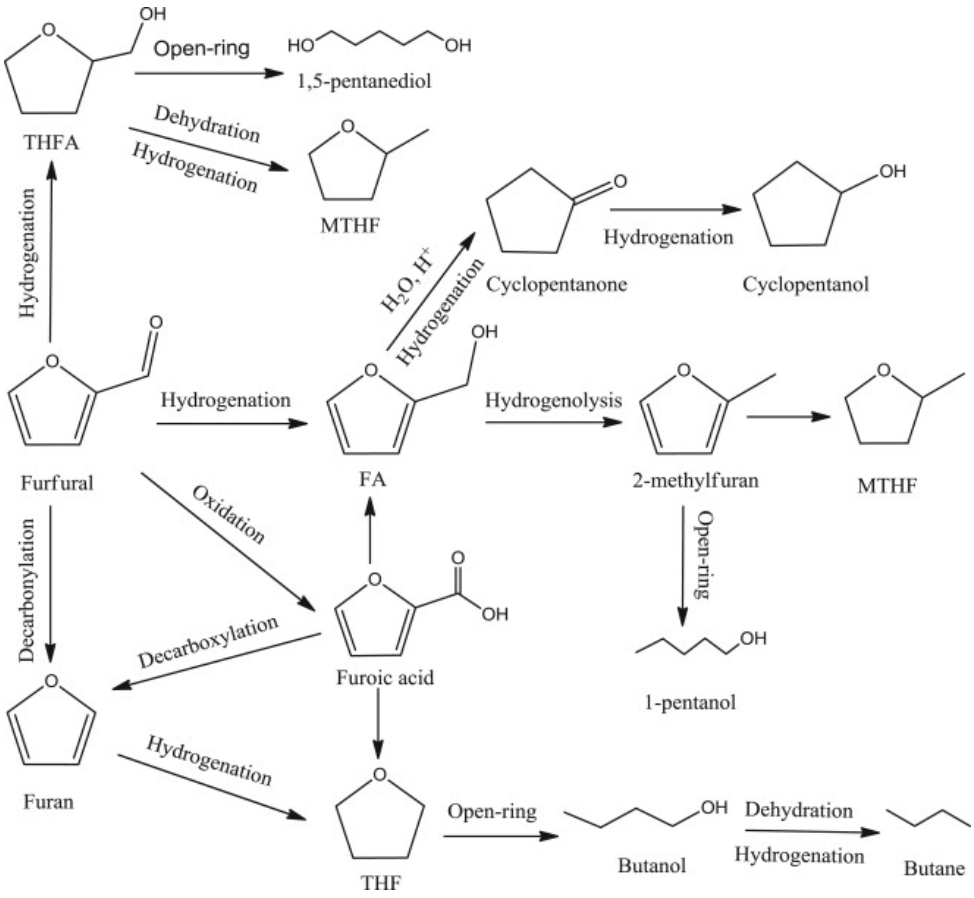

Figure 1. Pathways of furfural conversion to versatile chemicals.[12]

Heterocyclic aldehyde functional groups in furfural allow conversion to versatile chemicals such as polymers, fine chemicals, and bio-fuels.[10,13–15] Diverse reaction pathways from furfural to a wide range of chemicals can be seen in Figure 1.

Notably, furfural can be converted into tetrahydrofurfuryl alcohol (THFA), furan, tetrahydrofuran (THF), furfuryl alcohol (FA), 2-methylfuran (MF), methyl tetrahydrofuran (MTHF), etc.[12] FA is a colorless liquid used in resins or plastics manufacturing industries.[12] MF and MTHF are both colorless solvents that can be used for biofuels applications.[12] MTHF can

also be used in battery applications for electrolytes in secondary lithium batteries.[16]

Conventional thermo-catalytic methods for biomass hydrogenation operate at high temperatures ranging from 300 to 600 °C and require externally supplied hydrogen gas at high pressure.[17,18] On the other hand, electrocatalytic hydrogenation (ECH) is an emerging biomass conversion method that is preferred because it is safer and more environmentally friendly than conventional chemical hydrogenation. ECH can be operated at temperatures below 100°C, lower pressure because water is the atomic hydrogen source, and ECH can exploit electrons from renewable electricity.[14,19–24]

During ECH, water oxidizes to produce protons and generate electrons at the anode as shown in Equation 1.1. These proton and electron pairs are combined as adsorbed hydrogen at the cathode surface, typically through a Volmer mechanism as presented in Equation 1.2.[25]

$$\text{Water oxidation: } 2\,H_2O \rightarrow 4H^+ + 4e^- + O_2 \qquad (1.1)$$

$$\text{Volmer mechanism: } H^+ + e^- + * \rightarrow H^* \qquad (1.2)$$

These adsorbed protons can be consumed during furfural ECH or hydrogen evolution reaction (HER). As presented in Figure 2, furfural can be reduced to FA by two electrons along with two adsorbed hydrogens at the electrode surface. FA can be further reduced to 2-methylfuran by two electrons along with another two adsorbed hydrogens.

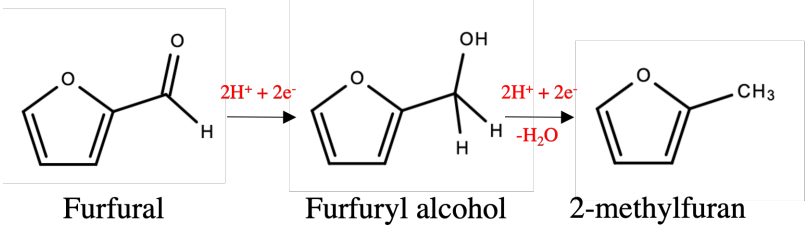

Figure 2. Furfural electrocatalytic hydrogenation pathways to furfuryl alcohol and 2-methylfuran.

Adsorbed hydrogen produced from Volmer reaction can also be consumed in HER.

Hydrogen gas can be produced via Tafel or Heyrovsky mechanism as presented in Equations 2.1 and 2.2.[25]

$$\text{Tafel mechanism: } H^* + H^* \rightarrow H_2 \qquad (2.1)$$

$$\text{Heyrovsky mechanism: } H^* + H^+ + e^- \rightarrow H_2 \qquad (2.2)$$

The Tafel reaction occurs when two adsorbed hydrogens at the electrode surface react to produce H_2. On the other hand, the Heyrovsky reaction takes place between adsorbed hydrogen and a proton in the electrolyte. These reactions lower the Faradaic efficiency (FE) of furfural ECH because they consume adsorbed hydrogens, which is required for furfural to be electrocatalytically hydrogenated.

Another possible side reaction is furfural electrodimerization. A proton and electron pair from bulk solution is consumed to convert furfural to a carbonyl radical as shown in Figure 3.

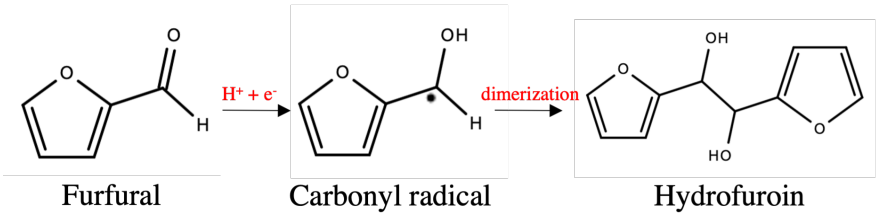

Figure 3. Schematic of electrodimerization of furfural to hydrofuroin.

The carbonyl radical can react with another radical to produce hydrofuroin and this reaction will lower FE of furfural ECH.[26]

Transition metals, such as copper and zinc have been studied for furfural ECH in various pH electrolytes.[22,24,27–30] Dhawan *et al*. studied zinc wire catalyst in acidic, basic, and neutral pH electrolytes.[25] As a result, higher ECH selectivity over HER was achieved in neutral pH electrolyte in which 0.5 M sodium bicarbonate was used. Catalyst materials were also varied, using copper, nickel, zinc in pH of 8.4 at – 0.7 V/RHE. It was found that the zinc catalyst

outperformed copper and nickel in furfural ECH selectivity over HER, resulting in 88 % furfural conversion with a 73 % FE for FA.[24] Xu *et al*. studied furfural ECH with copper catalyst on nitrogen doped carbon nanosheets in basic pH electrolyte.[30] Owing to its high electrochemically active surface area of 2261 cm^2, 99 % furfural conversion with a > 95 % FE for FA were reported.[30] Li *et al*. reported that the highest furfural ECH to FA and MF yield were obtained at pH of 5.0 and 1.0, respectively, with nickel catalyst.[22]

Jung et al. showed the impact of an applied potential and furfural concentration on furfural ECH mechanism.[31] It was reported that the low initial furfural concentration could increase the FE for FA and MF while promoting HER. However, higher furfural concentration promoted polymerization of furanic compounds.

Taylor *et al*. studied supported platinum nanoparticle catalysts for selective furfural ECH and found that catalytic activity and selectivity are dependent on Pt particle size.[20] Dhawan *et al*. electrodeposited zinc catalyst on bare zinc foil to synthesize 5.4 m^2/g zinc metal nanoparticles.[25] Higher conversion, yield, and FE of FA were observed with higher surface area nanoparticles than those with bare zinc foil.[25] This suggests that zinc nano catalysts could be used to increase the electrocatalytic activity by increasing the catalytic surface area.

Rotating disk electrode (RDE) measurements have commonly been used to assess catalytic activity.[23,32–35] By rotating the electrode in electrolyte, the centrifugal force induces electrolyte solution to flow up to the electrode surface perpendicularly as shown in Figure 4.

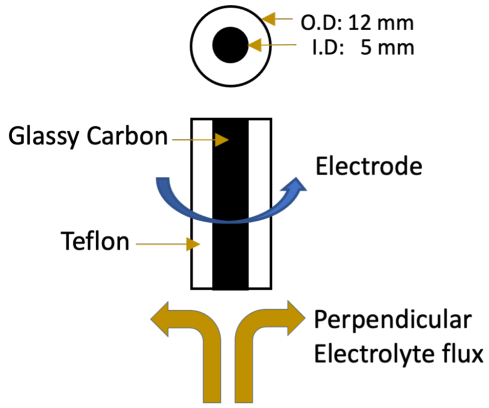

Figure 4. Schematic of rotating disk electrode.

This allows for steady-state mass transport to the electrode surface. Mass transport of solution can be controlled by changing the rotating speed of the electrode. Under mass transfer limited regime, kinetic parameters can be obtained from Koutecký-Levich analysis by varying the rotating speed.[36]

Chadderdon *et al*. used Cu RDE to perform cyclic voltammetry (CV) to determine the potential range for a furfural electrolysis in acidic (pH = 0.5) electrolyte.[26] Wang *et al*. implemented linear sweep voltammetry (LSV) using microparticle Cu RDE to compare onset potentials of HER and acetylene ECH.[37]

Glassy carbon RDEs can be modified by thin-film metal ink deposition using a drop casting method, to evaluate catalytic activity and kinetic parameters of the reaction with desired catalysts through electrochemical measurements under various rotating speeds. Suntivich *et al*. studied modified a thin-film RDE with perovskite transition submicrometer-sized metal oxides and Nafion binder to study the oxygen reduction reaction (ORR). To avoid oxide catalyst being dissolved due to the acidic nature of Nafion ionomer, they modified it to make alkali Nafion binder by neutralizing it in 0.1 M sodium hydroxide (NaOH).[34] Chourashiya *et* al. compared two ink preparation methods, ultrasonicating in water bath and ultrasonicating with rod directly in

ink, for ORR performance on platinum catalyst. They reported homogeneity of ink solution and evenly distributed catalyst on RDE are important factor of improving the electrocatalytic performance while minimizing the catalyst waste.[29]

Herein, we focused on modification of rotating disk electrodes using high surface zinc and copper metal nanoparticles. Scanning electron microscopy (SEM), energy dispersive spectroscopy (EDX), and Brunauer-Emmett-Teller (BET) analysis were carried out on commercial zinc and copper nanoparticles to confirm the morphology, chemical composition, and surface area. Various binders were studied to investigate a binder that would stably support metal nanoparticles without any film falling off the glassy carbon RDE during and after electrochemical measurements. Also, a selected binder would be able to allow catalysts to show higher electrocatalytic activities than our control electrodes. Zinc modified RDEs were optimized via binder-catalyst composition and total catalyst loading variations using cyclic voltammetry measurements. The kinetics of zinc modified RDEs for furfural reduction was studied through Koutecký-Levich analysis to derive the kinetic current densities, the number of electrons transferred in the reaction, and the Tafel slope.

2. Methods

2.1 Materials

2.1.1 Chemicals

Furfural (99 %) and glutaraldehyde solution (25 % in H_2O) were purchased from Sigma-Aldrich. Sodium bicarbonate ($NaHCO_3$, powder, 99.7 to 100.3 %), polyvinyl pyrrolidone (M.W. 40,000), and isopropyl alcohol (≥ 99.7 %) were purchased from Fischer Scientific. Polyvinyl alcohol (98-99 % hydrolyzed, high molecular weight), Nafion solution (Nafion® D-521 dispersion, 5 % w/w in water and 1-propanol, ≥ 0.92 meq/g exchange capacity), and ethylene glycol (≥ 99%) were purchased from Acros-Organics. Deionized water was purchased from VWR international and used for electrolyte and binder solution preparation. Sodium chloride (NaCl, ≥ 99%) was purchased from Columbus Chemical Industries. All materials were used as received.

2.1.2 Electrodes

Glassy carbon rotating disk electrodes (RDE) (AFE3T050GC, 0.5 cm diameter) purchased from Pine Research Instrumentation was used for the working electrode. Alumina slurries (0.05 μm, 0.3 μm, and 1 μm suspensions) were purchased from Buehler and used to polish disk electrodes. Zinc nano powder (≥ 99 %) and copper nano powder (≥ 99.5 %) obtained from Sigma-Aldrich were used as catalysts for RDE modification. A reversible hydrogen electrode was used as a reference electrode (RE). It was custom made with a Pt wire (99.95 %, 0.5 mm diameter) purchased from Thermo Fisher Scientific in a one-end sealed glass tube. The RE was prepared by filling the glass tube with electrolyte. Glass wool obtained from Supelco was inserted at the opened end of the tube to prevent any bubble buildup at the RE from Argon sparging. A graphite rod (2.5 cm diameter) purchased from Pine Research Instrumentation was used as a counter electrode (CE). The surface of the CE was cleaned with sandpaper (800 grit

(P2400), 6.5 μm diameter) purchased from Buehler to remove corrosion or oxidized metal on the surface, then rinsed with ethanol and deionized water prior to each experiment.

2.2 Experimental

2.2.1 Metal Nanoparticles Characterization

2.2.1.1 SEM

The morphology of commercial metal nanoparticles, binder films, and catalyst-binder films were characterized via images obtained from scanning electron microscope (SEM) JEOL JSM 6610LV. All specimens were gently mounted on stubs using adhesive carbon tabs. Non-conductive binder film samples were gold coated at 20 mA for 3 minutes using the Emscope sputter coater to make the sample conductive. An accelerating voltage of 10-12 kV with working distance (WD) of 10 mm and a spot size of 20-30 was used.

2.2.1.2 EDX

An energy dispersive x-ray (EDX) analysis was conducted to obtain elemental composition of metal particles using JEOL JSM 6610LV and Oxford AZtec software.

2.2.1.3 BET

Metal nanoparticles were degassed at 100 °C for 4 hours prior to BET surface area analysis. Surface area of samples were determined by N_2 adsorption-desorption at -196 °C under pressures from 0.1 to 0.99 relative to a N_2 saturation pressure, 760 mmHg using Micrometrics ASAP instrument.

2.2.2 Metal Ink Solution Preparation

To evaluate electrochemical measurements using rotating disk electrodes modified with metal nanoparticles, appropriate binders must be studied to adhere metal particles on the electrode surface throughout measurements under high rotating speeds.

Ink recipes using commonly-studied metal particle binders from literature were

investigated, using zinc nanoparticles. Ink recipes can be seen in Table 1 below.

Table 1. Ink recipes.

NP Film	Ink Recipe	Metal: Binder (wt%)
NP-Nafion[38]	20 mg NP + 100 ul 5 wt% Nafion Solution	81:19
NP-Nafion-EtOH[39]	4 mg NP + 150 ul ethanol + 50 ul 5 wt% Nafion solution	63:37
NP-Nafion-IPA[40]	5 mg NP + 170 ul DIW + 680 ul IPA + 150 ul 0.5 wt% Nafion solution	88:12
NP-PVP-EG[41]	1 g PVP in 100 ml EG + 10g NP	91:9
NP-PVP-EG-IPA[42]	NP + PVP + IPA + EG + DIW (=5:19:13:18:45 w/w)	21:79
NP-PVA[43]	2 wt% PVA solution + 92 wt% NP	92:8
NP-PVA-GA[44]	1 wt% GA in 2 wt% PVA solution + 92 wt% NP	92:8

Polyvinyl pyrrolidone (PVP) solution was prepared for NP-PVP-EG in 100 ml ethylene glycol (EG) for every 1 g of PVP for 2 hours under continuous stirring prior to mixing the solution with metal particles.[41]

For NP-PVP-EG-IPA ink solution, PVP, isopropyl alcohol (IPA), EG, and deionized water (DIW) were continuously stirred for 30 minutes prior to adding metal nanoparticles.[42]

2 wt% polyvinyl alcohol (PVA) solutions were prepared by dissolving PVA pellets in deionized water at 80 °C for at least 30 minutes under continuous stirring.[43] The PVA solution was cooled down to room temperature before use.

For each recipe, metal nanoparticles and other solvents including the binder solution were each measured with a micropipette. The solutions were vortexed vigorously for a minute using a vortex mixer (Thermolyne Maxi Mix II Variable Speed Control Type 37600 Mixer) followed by ultra-sonication in an ice-water bath for at least 10 minutes. This step was repeated once more to ensure dispersion of metal particles in solution.

2.2.3 Modified Rotating Disk Electrodes Preparation

Glassy carbon disk electrodes were polished with a water slurry of 1 μm, 0.3 μm, 0.05

μm Alumina in a figure eight pattern, rinsed with ethanol and deionized water, sonicated in deionized water to remove Alumina particles for 2 minutes between each polish, and dried at a room temperature.

For the catalytic electrode surface coating process, 8.6 mg_{metal} cm^{-2} were deposited on the polished glassy carbon disk electrode surface. Metal ink drop-casted electrodes were covered with a glass beaker and air-dried overnight.[45] After drying, thin film electrodes were visually inspected using a Nikon Eclipse LV150 microscope for a uniform ink deposition.

2.2.4 Electrochemical Cell Set up

A water jacketed reactor contained 50 ml of 0.5 M sodium bicarbonate ($NaHCO_3$) as an electrolyte for hydrogen evolution reaction (HER) measurements and 100 mM furfural was added in the electrolyte for electrocatalytic hydrogenation (ECH) measurements of furfural. The temperature of the cell was controlled at 25 ± 0.1°C using a water jacket. Electrolyte pH was measured at 8.4 ± 0.1 using a pH meter (Fisher Scientific, Accumet Basic AB15) and was purged with Argon for a minimum of 15 minutes prior to each experiment to keep the electrolyte deoxygenated. A three-electrode system was used in the electrochemical cell with a modified RDE as the working electrode, reversible hydrogen electrode (RHE) as the reference electrode, and a graphite rod as the counter electrode. An electrode rotator (Pine Research, MSRX Speed Control) was used to control the rotating rate of the working electrode. The electrochemical cell was connected to a potentiostat (VSP, Bio-logic) which was controlled with the EC-lab software.

2.2.5 Electrochemical Measurements

Cyclic voltammetry (CV) was performed in the absence and presence of furfural in electrolyte between -1.0 V to -0.6 V/RHE at a scan rate of 20 mVs^{-1} at 1600 rpm using modified RDEs. Current densities at the third CV cycle were compared to optimize metal electrode

conditions.

Chronoamperometry (CA) was carried out post CV at -0.7 V/RHE at 1600 rpm for 30 minutes to study the stability of modified electrodes using various binders by measuring the current change over time. CA was also used to obtain steady-state current densities at various rotating speeds and various potentials to study kinetic parameters through Koutecký-Levich analysis modified RDEs. Measurements were obtained at the order of rotating rates of 1600, 900, 625, 330, 220, 140, and 100 rpm. RDEs were rotated from 1600 to 100 and back to 1600 rpm.

2.2.6 Swelling Degree Measurement

2 wt% PVA solution and 1 wt% glutaraldehyde (GA) in 2 wt% PVA solution were each dried in oven at 104 °C overnight.[46] The weight of each dried films was measured as W_i and immersed in 50 mL DIW for 24 hours. The films were then removed from the water and any excess water was removed using the filter paper. Swollen weights are measured as W_f. The swelling degree was then calculated by[46] :

$$\text{Swelling Degree (\%)} = \frac{Wf - Wi}{Wi} \times 100 \qquad (3)$$

2.2.7 Koutecký-Levich Analysis

Kinetics of furfural electrocatalytic hydrogenation were studied using zinc-modified rotating disk electrodes through Koutecký-Levich plot. The kinetic current density and number of electrons transferred (n) can be derived using the Equations 4.1 – 4.3 below for Koutecký-Levich analysis[47]:

$$\frac{1}{i} = \frac{1}{i_k} + \frac{1}{i_d} \qquad (4.1)$$

$$i_d = B \cdot n \cdot \omega^{0.5} \qquad (4.2)$$

$$B = 0.62 \cdot F \cdot D^{\frac{2}{3}} \cdot \nu^{-\frac{1}{6}} \cdot C \qquad (4.3)$$

where i, i_k , i_d , measured current density, kinetic current density, and limiting current

density, respectively. Limiting current density is dependent on the rotating speed of the electrode (ω), n and a constant B, which is determined by the Faraday's constant (F = 96,485 C mol^{-1}), surface area of the electrode (A), diffusion coefficient ($D = 1.13 \times 10^{-9}$ m^2/s)[48] of furfural in solution, kinematic viscosity of solution ($\nu = 1.13 \times 10^{-6}$ m^2/s)[49], and concentration of furfural in the electrolyte (C). A Koutecký-Levich plot (i^{-1} vs. $\omega^{-0.5}$) at various rotating speeds can be fitted to derive i_k and n using the y-intercept and the slope of the plot, respectively. Example calculations are available.[50]

2.2.8 Tafel Slope Analysis

Tafel slope analysis of nano zinc modified electrodes was performed to study rate of ECH on electrode surface relating to the overpotential. Tafel equation can be derived from the Butler-Volmer equation as presented below where i_0 is the exchange current density (mA/cm^2), α_α and α_c are anodic and cathodic transfer coefficients respectively. η_s represents surface overpotential (V), R represents the gas constant (8.314 J/mol K), and T represents the temperature.[36]

$$\text{Butler-Volmer equation: } i = i_0 \left[exp\left(\frac{\alpha_\alpha F \eta_s}{RT}\right) - exp\left(\frac{\alpha_c F \eta_s}{RT}\right)\right] \qquad (5)$$

The exponential terms represent the anodic and cathodic current, respectively and one term can be ignored when the other reaction is dominant. Further, η_s can be expressed in terms of the current in base$_{10}$ logarithm terms as presented in equations 6.1 and 6.2 below. Finally, i_0 and b (Tafel slope, mV/dec) can be obtained from a Tafel plot (η_s vs. i).[36] Example calculations are available.[50]

$$\eta_s = a + b \log_{10} i_k \qquad (6.1)$$

$$a = \frac{-2.303\,RT}{\alpha_c F} \log_{10} i_0,\ b = \frac{2.303\,RT}{\alpha_c F} \qquad (6.2)$$

3. Results and Discussion

In this research, zinc nanoparticles were considered for binder optimization, electrode optimization, and Koutecký-Levich analysis. Copper nanoparticles were studied for current density decay rate comparison between different catalysts, and polarization curve comparison.

3.1 Zinc and Copper Nanoparticles Characterization

Commercially produced zinc and copper nanoparticles were characterized by scanning electron microscopy (SEM) and energy dispersive x-ray (EDX) to analyze the morphology and elemental compositions before making the electrode. Figures 5a and 5b below present SEM images of commercial zinc and copper nanoparticles, respectively. Spherical morphologies are shown for both zinc and copper, suggesting a higher surface area than bulk metals for ECH.

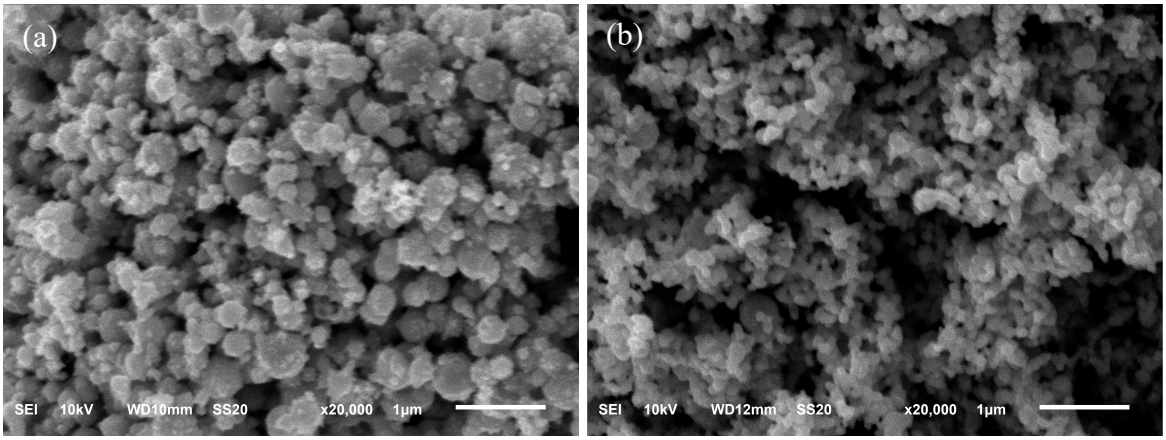

Figure 5. SEM images of (a) zinc nanoparticles (b) copper nanoparticles.

The EDX spectrum of metal zinc and copper nanoparticles spectrum can be seen in Figure 6, which revealed 91 wt% Zn and 9.4 wt% O in zinc particles and 94 wt% O: 6.2 wt% in copper particles. These confirms that the nanoparticles used in this study are nearly-pure zinc and copper.

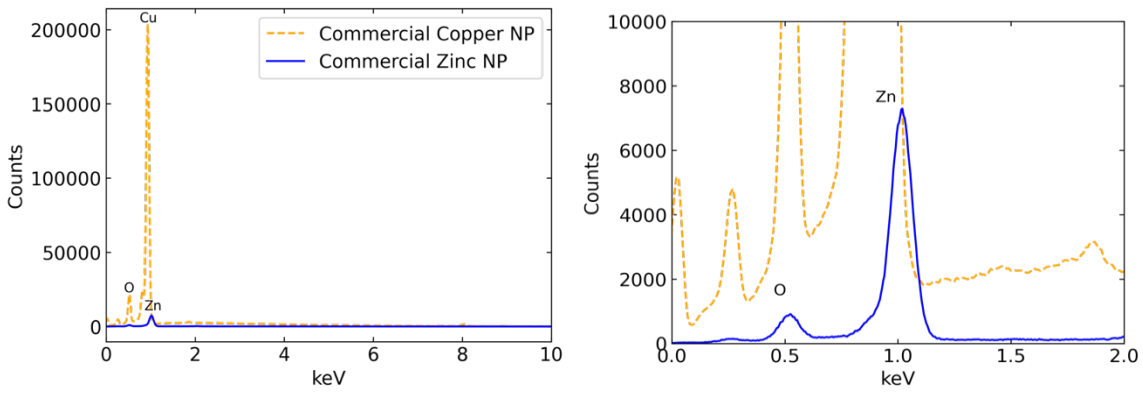

Figure 6. EDX spectra of commercial zinc and copper nanoparticles.

BET analysis was conducted on both zinc and copper nanoparticles. Surface area was analyzed and is presented in Table 2 below. The table also includes surface area per mass of electrodeposited zinc nano particles from literature[25], and calculated zinc foil and wire. These comparisons indicate that nano particles offer higher surface area per mass than bulk metals, leading to greater availability of electrocatalytic active sites.

Table 2. Surface area of zinc and copper nanoparticles, electrodeposited zinc, zinc foil, and zinc wire.

	Surface area per unit mass (m^2/g)
Zinc nanoparticle	5.0
Copper nanoparticle	5.6
Electrodeposited zinc[25]	5.4
Calculated macroscopic zinc foil	10^{-3}
Calculated macroscopic zinc wire	8.8×10^{-4}

3.2 Electrode Modification and Binder Performance

For electrochemical measurements of modified rotating disk electrodes, various binders were studied as binders for zinc nano powders on rotating glassy carbon disk electrodes. Mainly, Nafion®, polyvinyl pyrrolidone (PVP), and polyvinyl alcohol (PVA) were compared in terms of

stability. Modified RDEs were prepared using recipes in Table 1 above.

Microscopic images of modified electrode surface before and after the stability test performed in hydrogen evolution reaction (HER) conditions are presented in Figure 7 below.

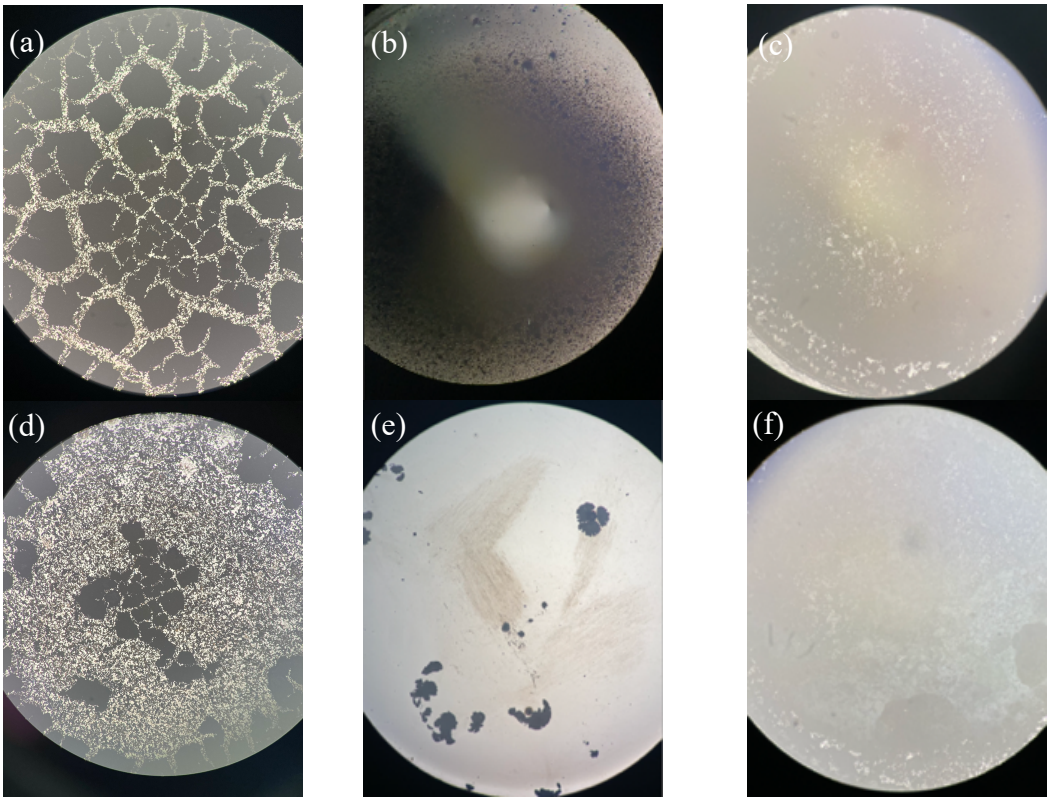

Figure 7. (a) Zn-Nafion (b) Zn-PVP-EG-IPA (c) Zn-PVA before and (d) Zn-Nafion (e) Zn-PVP-EG-IPA (f) Zn-PVA after stability test in $NaHCO_3$ viewed through an optical microscope.

NP-Nafion ink solution resulted in homogeneous ink solution with uniform ink deposition on blank glassy carbon electrode surface. However, as the ink was completely dried, observable cracks formed as shown in Figure 8.

Figure 8. Zn-Nafion RDE after drying.

The cracks after drying process were also viewed through optical microscope as shown in Figure 7a. These cracks on the electrode surface are consistent with previous literature.[51–55] It has been suggested that the tensile stress within the catalyst film during drying process could result in film cracking.[55] However, the film was stable enough to resist peeling after the electrode surface was gently washed with deionized water.

Additionally, weak adhesion of metal particles to the glassy carbon electrode surface was observed as shown in Figure 7d after three cycles of CV (cyclic voltammetry) in the absence of furfural. This indicates that Nafion is not suitable as a stable binder for zinc nanoparticles on glassy carbon.

The Nafion binder were was also studied using other solvents. NP-Nafion-EtOH solution includes ethanol and NP-Nafion-IPA ink solution includes isopropyl alcohol in ink solution. Homogeneous metal suspensions were not achieved using either method, as shown in Figures 9a and 9b. Therefore, it was concluded that Nafion solution is not a good choice of binder for zinc nanoparticles because non-homogeneous ink will form unevenly distributed films.

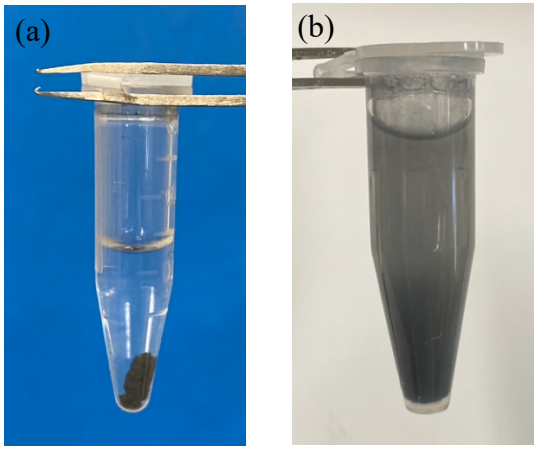

Figure 9. Non-homogeneous ink solutions (a) Zn-Nafion-EtOH (b) Zn-Nafion-IPA.

PVP was investigated as a hydrophilic binder option to enhance the homogeneity of

catalyst ink and to achieve thin film deposition. Homogeneous and non-viscous ink was obtained using NP-PVP-EG ink method and zinc nanoparticles. Because the electrode is recommended to be kept in a temperature range between 10 °C to 25 °C and to keep the ink drying method consistent as other methods, the NP-PVP-EG electrode was dried overnight at a room temperature.[56] However, with the presence of ethylene glycol (EG) as a solvent in the ink, it required a much longer time to obtain a flat electrode surface. A dome-like surface was observed after 20 hours of drying indicating that the EG was not completely evaporated due to its low evaporation rate. After CV scans at 1600 rpm, the center of the dome-like electrode surface was "dented" suggesting that the film was not fully dried. The formation of a dent after rotating the electrode in electrolyte could be due to the convective force of fluid flow at the electrode surface.

Isopropyl alcohol (IPA) was added to the PVP ink to improve the evaporation rate.[42] The presence of IPA and a lower EG concentration of 18 wt% (compared to 91 wt% in NP-PVP-EG) assisted in obtaining a thin film after drying overnight. However, as observed in Figure 6b, the nanoparticles were not evenly distributed on the electrode surface. This could be due to change in viscosity of the ink during the drying process affected by the IPA evaporation.[57] A high PVP concentration of 19 wt% may have lead the ink to be viscous as well. Nonetheless, it was found that the PVP binder was not stable. Figure 7e represents the Zn-PVP-EG-IPA surface after three CV scans in HER conditions. Almost the entire film was removed, indicating a poor binding performance and suggesting that lower PVP binder solution will result in much poorer binding behavior, despite its reduced ink viscosity.

PVA was studied as a second hydrophilic binder option. PVA is a water-soluble molecule with hydroxyl groups on every repeating unit, offering hydrogen bonding sites.[58] For this reason, Sun *et al*. and Rajeswari *et al*. used PVA as a strong binder to achieve high adhesion strength

between active materials and the electrode surface.[58,59] Studies have shown that zinc oxide nanoparticles doped in a PVA matrix through the interaction between zinc ions and hydroxyl group of PVA resulted in strong hydrogen bonding.[60] Zinc nanoparticles was well dispersed in 2 wt% PVA solution to form a Zn-PVA ink. Homogeneous ink solution was obtained and a thin Zn-PVA film was deposited on glassy carbon electrode. Binder stability tests were performed with Zn-PVA RDE via three CV scans in HER conditions. Figures 7c and 7f represent the Zn-PVA RDE surface before and after the stability test, respectively.

Visual analysis on Zn-PVA RDE surface suggests PVA acts as a stable binder because almost all the content deposited before the stability test remained on the electrode surface after the stability test at 1600 rpm.

SEM analysis of zinc and copper electrodes modified with PVA was performed to detect any change in morphology due to the binder, before the stability test. Figures 10a through 10c reveal zinc and copper nanoparticles bound by PVA binder, respectively. It can also be observed that the spherical morphologies are intact even after the metal ink RDE modification process.

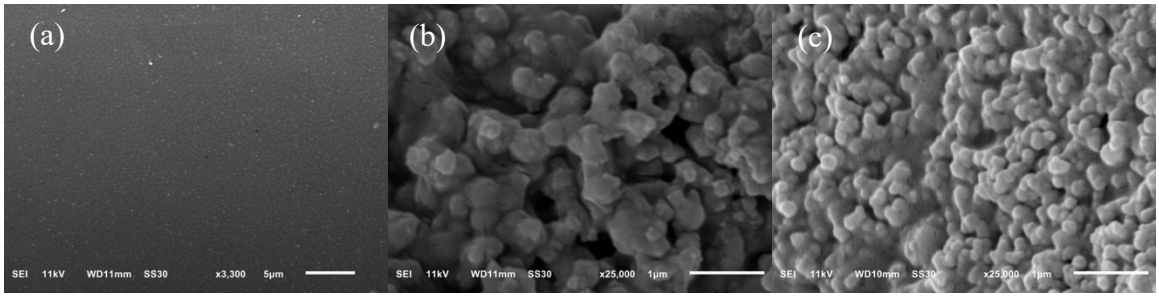

Figure 10. SEM images of (a) PVA (b) Zn-PVA (c) Cu-PVA films.

Chronoamperometric (CA) measurement in Figure 11 demonstrates Zn-PVA RDE stability in HER condition. Unlike other modified electrodes, continuous current densities were observed throughout the 10-minute CA for both PVA film itself and Zn-PVA film.

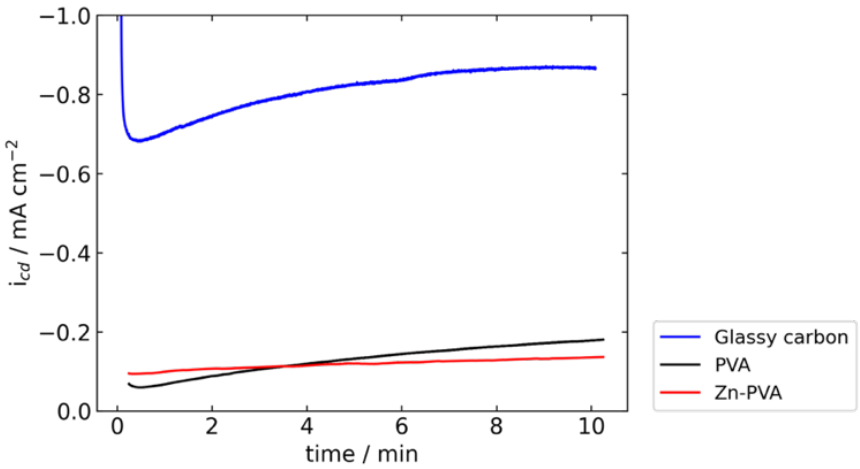

Figure 11. Stability test of Zn-PVA RDE at constant potential -0.7 V/RHE (Argon sparged 50 ml 0.5 M $NaHCO_3$ at T = 25 °C, 1600 rpm, pH = 8.4).

This could be due to good film adhesion to the glassy carbon electrode surface. These CA results were compared to the CA behavior with glassy carbon electrode at the same condition. If the modified ink was unstable, the films would be partially or fully removed, and the glassy carbon would act as a catalyst, giving higher current densities for HER as represented in Figure 11.

It is also important to consider the catalytic activities for both HER and ECH. The third CV cycle with each electrode are compared in Figure 12.

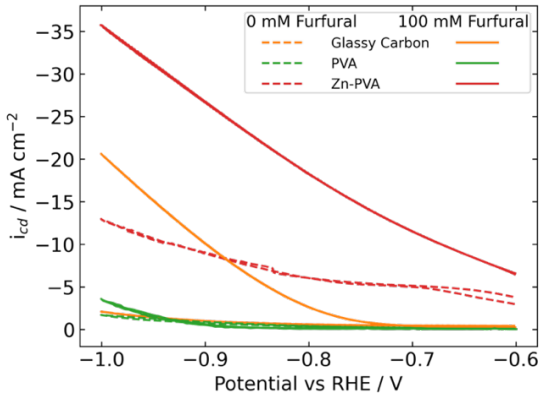

Figure 12. CV for HER (dashed line) and furfural ECH (solid line) on various electrodes (Argon sparged 50 ml 0.5 M $NaHCO_3$ at T = 25 °C, 1600 rpm, pH = 8.4).

It was observed that both PVA and Zn-PVA resulted in lower HER current densities compared to glassy carbon. This suggests that the PVA binder suppresses HER. Additionally, current densities for furfural ECH with PVA RDE is lower than that with glassy carbon. It suggests that the ECH is suppressed with the addition of PVA on glassy carbon. However, ECH activities with Zn-PVA are greater than glassy carbon. This indicates that the zinc is a better catalyst material than glassy carbon for furfural ECH.

As a result, PVA outperformed other binders studied in this paper for stability, as shown in CA measurements, and improved ECH performance as shown by CV measurements. Therefore, PVA was selected as the nanoparticle catalyst binder for further electrocatalysis measurements.

3.3. Zn-PVA Ink Optimization

As it was observed earlier that the PVA film suppressing ECH activity, zinc composition and total zinc loading were varied to optimize Zn-PVA. Catalytic activities in the presence of 100 mM furfural and at -0.7 V/RHE were compared using the cyclic voltammetry technique.

3.3.1 Zinc Composition

Zinc composition in the electrode varied from 88 wt% to 96 wt%, with the balance made up by PVA, while keeping total zinc loading constant at 6.1 $mg_{Zn}\,cm^{-2}$. Respectively, therefore, PVA solutions of concentrations varying from 3.3 wt% to 1.0 wt% were prepared. This allowed us to retain ink on the glassy carbon RDE, and avoid overflowing the disk.

ECH for varied zinc composition were studied by comparing the current densities of the third CV cycle at -0.7 V/RHE as shown in Figure 13.

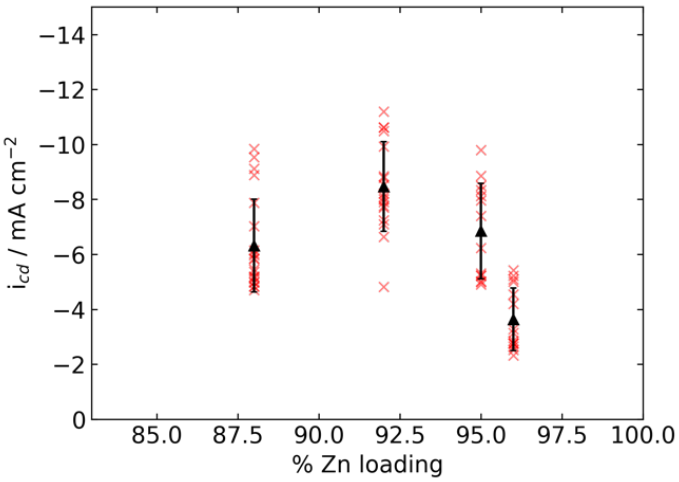

Figure 13. Current densities on Zn-PVA RDE at various zinc compositions at -0.7 V/RHE (Argon sparged 100 mM furfural in 50 ml 0.5 M $NaHCO_3$ at T = 25 °C, 1600 rpm, pH = 8.4).

Current densities increased from 88 wt% to 92 wt% then dropped gradually as more catalyst was loaded. This suggests that binder to catalyst ratio affects the binding stability to hold the catalysts thus affecting the catalytic activity.

3.3.2 Zinc Loading

Varying total zinc loading also had an effect on catalytic activities for furfural ECH. Fixing the zinc content at 92 wt%, total zinc loading was varied from 3.1 to 11 $mg_{Zn}\,cm^{-2}$. As shown in Table 3, the Zn-PVA film thickness was assessed visually after drying overnight at room temperature.

Table 3. RDE surface with varying zinc loading after drying.

Total Zn loading (mg_{Zn} cm^{-2})	**3.1**	**4.9**	**6.1**	**8.6**	**11**
					

These images show an increasing thickness of the Zn-PVA film with total zinc loading. Similar to the zinc content optimization, current densities at two potentials for varying total zinc loading were measured as shown in Figure 14.

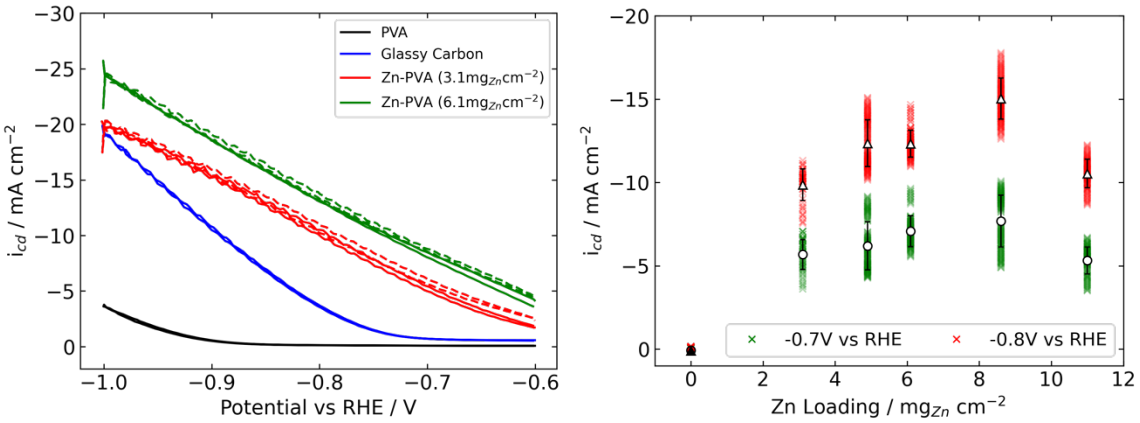

Figure 14. Current densities on Zn-PVA RDE at various total zinc loading at -0.7 V/RHE (Argon sparged 100 mM furfural in 50 ml 0.5 M $NaHCO_3$ at T = 25 °C, 1600 rpm, pH = 8.4).

At – 0.7 V/RHE, there was not a significant current density dependence on zinc loading. However, a trend of current density increasing with zinc loading was observed up to 8.6 mg_{Zn}/cm^2, above which a decrease is observed. The decrease in current density may be due to catalyst from a thicker film falling off due to decreased PVA binding performance. Current densities were compared again at a lower potential, -0.8 V/RHE. At this potential, a similar trend was observed. However, the variation in current density is more significant. As a result, a loading of 8.6 mg_{Zn}/cm^2 showed maximum ECH current densities. Therefore, 92 wt% 8.6 mg_{Zn}/cm^2 was determined to be our optimized electrode design for the glassy carbon RDE.

3.4 PVA Crosslinking with Glutaraldehyde

After a three-cycle CV scan, a 30 minute chronoamperometry (CA) study was conducted to observe current density behavior over time. The effect of crosslinking on current density decay was studied by crosslinking PVA with glutaraldehyde (GA). Hydroxyl groups from PVA react with glutaraldehyde to form a strong acetal group.[44] This could potentially improve the PVA binder stability because fewer hydroxyl groups from PVA will react with water in the electrolyte, leading to a reduced swelling.

The swelling degree of films of pure PVA and PVA crosslinked with 1 wt% GA were

first observed, and they were 370 ± 33 % and 330 ± 8.7 % respectively. These swelling degrees are consistent with previous literature.[46] It was observed that the swelling degree had decreased modestly with the addition of glutaraldehyde. SEM images in Figure 15a and 15b compare the modified electrode surface between Zn-PVA and Zn-PVA-GA films, and suggest minimal change in morphology.

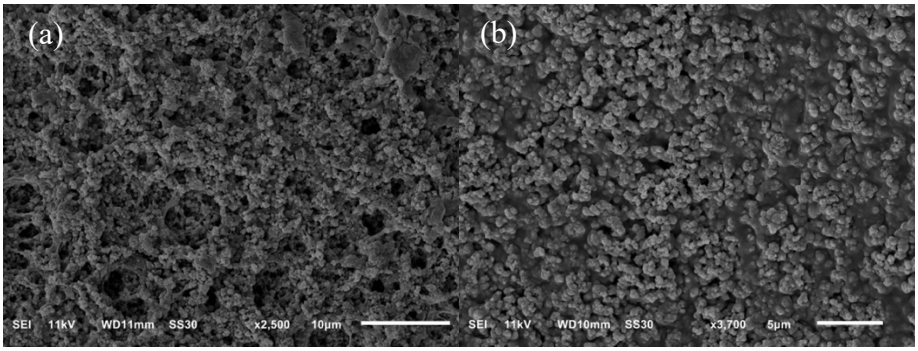

Figure 15. SEM image of (a) Zn-PVA (b) Zn-PVA-GA.

CA measurements were conducted at -0.8 V/RHE in furfural after three CV cycles for Zn-PVA, Zn-PVA-GA, Cu-PVA, Cu-PVA-GA films, to analyze the overall current densities and the current density change over time, as shown in Figure 16.

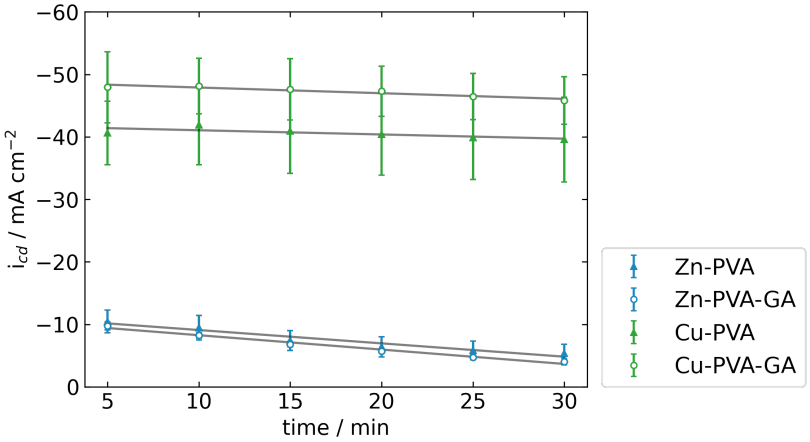

Figure 16. Current density decay rate comparison between Zn-PVA, Zn-PVA-GA, Cu-PVA, Cu-PVA-GA at -0.8 V/RHE (Argon sparged 100 mM furfural in 50 ml 0.5 M $NaHCO_3$ at T = 25 °C, 1600 rpm, pH = 8.4).

With the addition of glutaraldehyde on zinc catalyst, lower current densities were observed with a similar rate of decay as the uncrosslinked film. Lower current densities could be due to a tighter polymer structure or increased hydrophobicity from crosslinking effect, lowering the number of active sites available for electrocatalysis. On the other hand, higher current densities were observed with the addition of glutaraldehyde to the copper-catalyzed electrode. Also, it was interesting to observe overall higher current densities with copper catalyst compared to zinc, which is the opposite observation by Dhawan *et al*.[24] This could be due to a decrease in local pH from addition of PVA binder, favoring copper over zinc in furfural ECH. Therefore, polarization curves of copper nanoparticles were compared with zinc nanoparticles for both ECH and HER, as discussed below.

A straight line was used to fit the current density variation with time from Figure 16, to evaluate the decay rate. Table 4 below shows the percentage current density change over time for Zn-PVA, Zn-PVA-GA, Cu-PVA, and Cu-PVA-GA to see the effect of crosslinking on current density decay rate.

Table 4. Percentage current density change over time.

	Zn-PVA	**Zn-PVA-GA**	**Cu-PVA**	**Cu-PVA-GA**
$\frac{\%_{icd}}{min}$	2.0 ± 0.52	2.4 ± 0.33	0.17 ± 0.14	0.20 ± 0.067

It was found that the percentage current density changes over time increased with the addition of glutaraldehyde with both zinc and copper catalysts. This indicates that crosslinking did not help enhance the stability of the binder. However, percentage current density changes over time with Cu-PVA and Cu-PVA-GA are significantly smaller than with Zn-PVA and Zn-PVA-GA. Copper showed more stable behavior over time compared to zinc. This suggests that the PVA film stability over time differs with different catalysts.

3.5 Polarization Curve

Furfural ECH and HER polarization curves were obtained with Zn-PVA, Zn-PVA-GA, Cu-PVA, and Cu-PVA-GA in 0.5 M $NaHCO_3$ at 25 °C. Faradaic efficiency (FE) calculations were conducted at each condition as well by taking the ratio between ECH and HER current densities as follows:

$$FE_{ECH} = \left(1 - \frac{i_{HER}}{i_{ECH}}\right) \times 100(\%) \qquad (7)$$

Overall polarization curves and FE are shown in Figure 16 for zinc and copper electrodes modified with 92 wt% metal at 8.6 $mg_{catalyst}/cm^2$.

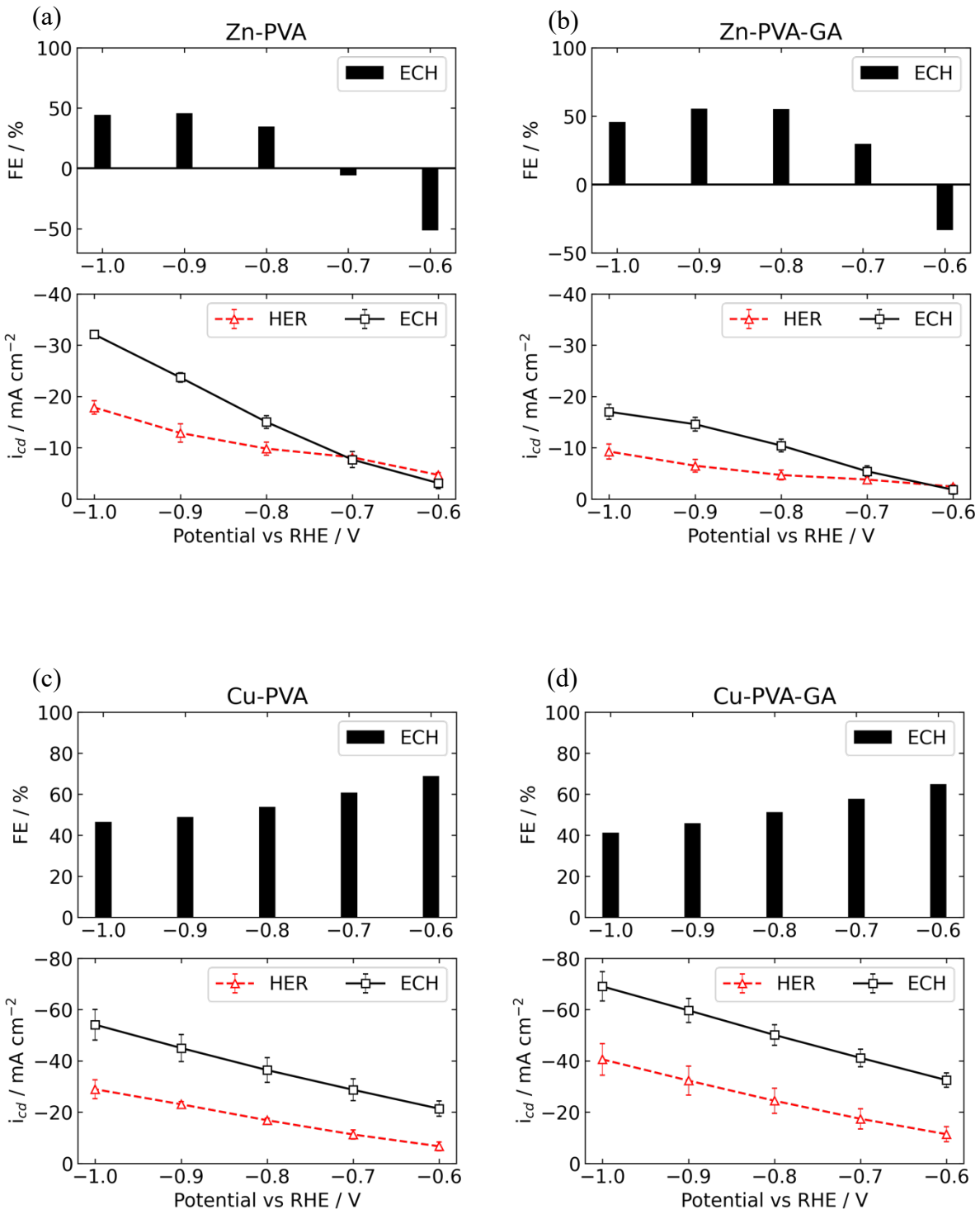

Figure 17. Furfural ECH and HER polarization curves and Faradaic efficiencies with (a) Zn-PVA (b) Zn-PVA-GA (c) Cu-PVA (d) Cu-PVA-GA in 50 ml 0.5 M $NaHCO_3$ (Argon sparged at T = 25 °C, 1600 rpm, pH = 8.4).

Current densities increased with the addition of furfural in electrolyte on all electrodes except for Zn-PVA at -0.6 and -0.7 V/RHE, and Zn-PVA-GA at -0.6 V/RHE. With Zn-PVA, ECH FE of 45.7% was obtained at -0.9 V/RHE. With Zn-PVA-GA, ECH FE of 55.5% was obtained at -0.9 V/RHE. On the other hand, ECH FE decreased with the increase of over potential when copper was used as a catalyst. Therefore, it can be suggested that the lower overpotential should be applied for copper for a higher furfural conversion selectivity. Similar to what was observed in ECH, GA crosslinked PVA showed a different behavior between zinc and copper in HER. With zinc, both HER and ECH current densities decreased with addition of GA. However, both HER and ECH current densities increased with addition of GA on copper. These different behavior between zinc and copper could be explained by their HER current densities. It could be suggested that at these over potentials, copper tends to be a better catalyst for HER.

3.6 Koutecký-Levich Analysis

Electrocatalytic current densities measurements with modified RDEs were conducted at various rotating speeds to calculate kinetic current densities and number of electrons transferred via Koutecký-Levich analysis. The dependence of current density on rotation speed also provides an estimate of the numbers of electrons transferred through the reaction. Copper was not used for this study because at lower rotation speeds, big hydrogen bubbles appeared, leading to an unstable noisy response. For this analysis, current densities were obtained with Zn-PVA and Zn-PVA-GA RDEs at various rotating speeds and applied potentials. The linear relationship between i^{-1} and $\omega^{-0.5}$ at potentials from - 0.7 V to -1.0 V/RHE are presented in Figure 18.

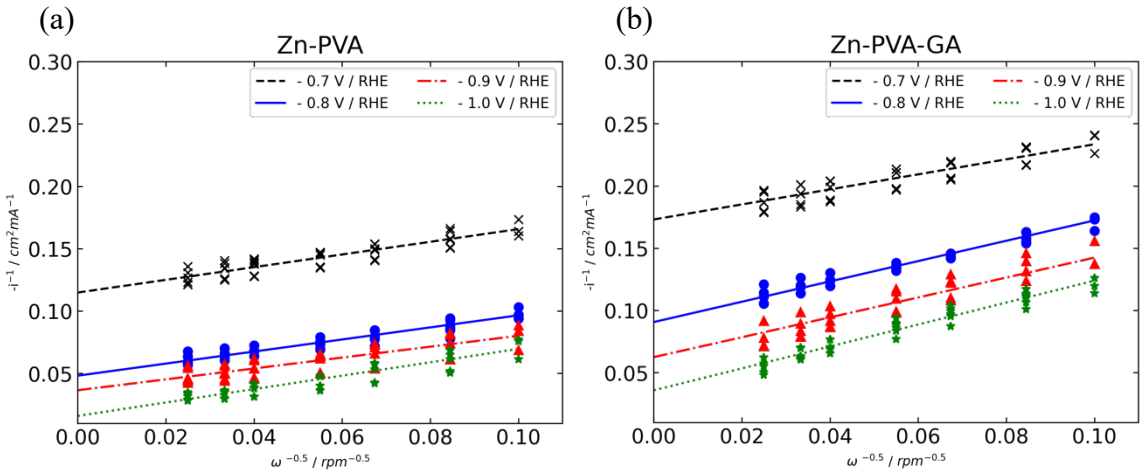

Figure 18. Koutecký-Levich plots at various potentials on (a) Zn-PVA and (b) Zn-PVA-GA RDE (Argon sparged 100 mM furfural in 50 ml 0.5 M NaHCO3 at T = 25 °C, pH = 8.4).

Increased current densities were observed with increasing rotating speeds on both modified electrodes at all potentials. This indicates the presence of mass transfer limitations. To compare the current densities where mass transfer limitation can be ignored, these plots at each potential were linearly extrapolated. As a result, kinetic current densities can be obtained from the y-intercepts of Figure 18 using the Koutecký-Levich equations 4.1 – 4.3. Kinetic current densities increased with the increase of over potential. This indicates that the reaction involves kinetically controlled ECH reaction.

With knowledge of the reactant diffusivity, the number of electrons transferred in reaction can be solved from the slope of linear plots in Figure 17. The number of electrons obtained with Zn-PVA and Zn-PVA-GA are presented in Table 5 below. Calculations are given in Appendix B.

Table 5. Number of electrons transferred at Zn-PVA and Zn-PVA-GA at various potentials (Argon sparged 100 mM furfural in 50 ml 0.5 M $NaHCO_3$ at T = 25 °C, pH = 8.4).

	-0.7 vs RHE / V	**-0.8 vs RHE / V**	**-0.9 vs RHE / V**	**-1.0 vs RHE / V**
Zn-PVA	2.4 ± 0.07	2.6 ± 0.11	2.8 ± 0.06	2.3 ± 0.12
Zn-PVA-GA	1.9 ± 0.01	1.6 ± 0.02	1.4 ± 0.04	1.4 ± 0.06

As mentioned above, respectively 1,2, and 4 electrons are required for furfural conversion to hydrofuroin, furfuryl alcohol, and 2-methylfuran. With Zn-PVA, at all potentials measured, n of 2.3 to 2.8 was obtained. This suggests that possible reaction pathways at Zn-PVA at these potentials involve furfural ECH to furfuryl alcohol and 2-methylfuran. Next, with Zn-PVA-GA, $1 < n < 2$ were obtained. This suggests a mixed reaction mechanisms of furfural conversion to both hydrofuroin and furfuryl alcohol

3.7 Tafel Slope Analysis

Tafel slope analysis was conducted on Zn-PVA and Zn-PVA-GA in presence of furfural to obtain Tafel slope (b) as well as the exchange current density (i_0) using equation 8.2 above, which helps understand the ECH performance of the electrodes. Tafel plot on Zn-PVA and Zn-PVA-GA in furfural ECH is presented in Figure 19 below.

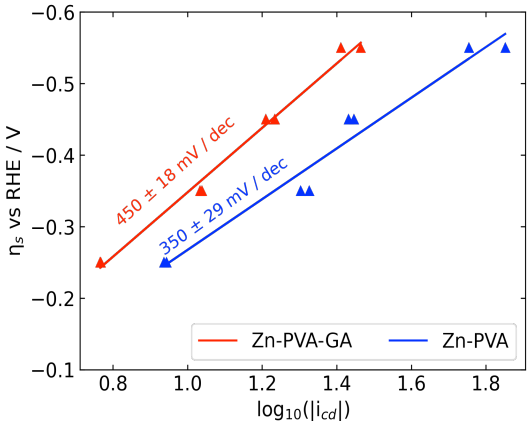

	Zn-PVA	**Zn-PVA-GA**
i_0(mA / cm²)	1.8 ± 0.04	1.7 ± 0.07
b (mV / dec)	350 ± 29	450 ± 18

Figure 19. Exchange current densities and Tafel slopes at Zn-PVA and Zn-PVA-GA.

Tafel slopes obtained on Zn-PVA and Zn-PVA-GA are 350 ± 29 and 450 ± 18 mV/dec, respectively. Lower Tafel slope is preferred as it indicates that less overpotential is needed for higher catalytic activity. Therefore, the results indicate that a Zn-PVA requires less overpotential than Zn-PVA-GA for furfural ECH. i_0 obtained on Zn-PVA and Zn-PVA-GA are 1.8 ± 0.04 and 1.7 ± 0.07 mA/cm^2, respectively.

3.8 Future Direction: Product Analysis

In order to quantitatively analyze the Faradaic efficiency(FE) of furfural ECH to furfuryl alcohol, 2-methylfuran, and hydrofuroin, a transition of an electrochemical set up from an undivided cell to an H-type cell is suggested. In a divided cell set up, the anode and cathode can be separated by a Nafion 115 cation exchange membrane. Additionally, 0.2 cm^2 glassy carbon RDE can be replaced with 5 cm^2 coiled zinc wire (1.56 mm diameter) to increase the product yield. Zinc can be used as a substrate for the optimized Zn-PVA electrode designed in this research. This will help understand the furfural reduction mechanism relating to the number of electrons observed from Koutecký-Levich analysis performed.

4. Conclusion

Electrocatalytic hydrogenation (ECH) is emerging as an environment friendly process to selectively convert biomass at a mild operating condition to value-added chemicals. Electricity from renewable energy can be used to split water from electrolyte to produce protons and electrons. These protons and electrons then used for electrolysis.

To study catalytic activities of nano catalyst using RDE, binders were studied and their different binding performances after three cycles of CV were compared. Polyvinyl alcohol (PVA) binder was determined to be the most stable binder that can withstand hydrogen bubble build-up on the electrode surface. Zn-PVA RDE showed higher catalytic activities when furfural was added in electrolyte, indicating Zn-PVA film enabled catalytic furfural ECH.

Next, Zn-PVA RDE was optimized by varying the binder composition and total zinc catalyst loading to achieve higher current densities than the glassy carbon electrode (GCE) which was the control electrode of this study. Too much binder content hindered catalytic activity, but enough binder was needed to support the nanoparticles on GCE. The highest catalytic current density was observed with 92 wt% 8.6 $mg_{catalyst}/cm^2$ RDE at -0.8 V/RHE. Glutaraldehyde (GA) was implemented to study the effect of crosslinking on current density decay rate. Zinc and copper showed a different behavior when it comes to stability over time. Current density stability improved by crosslinking PVA with GA on copper, whereas it did not on zinc. With Zn-PVA and Zn-PVA-GA RDE, the ECH was favored over HER at -0.9 V/RHE and achieved 46 % and 56 % FE ECH respectively based on current densities.

The kinetics of furfural ECH on zinc modified RDEs were studied via Koutecký-Levich analysis. Higher current densities were observed as the rotation was increased indicating the presence of mass transfer limitation. Kinetic current densities increased with decreasing

potential. Furthermore, number of electrons observed on Zn-PVA and Zn-PVA-GA were $2 < n$ and $1 < n < 2$, respectively, suggesting possible side products for furfural ECH.

Overall, this research will provide insight into optimized zinc nanoparticle electrode design on glassy carbon using PVA as a binder. For future directions, incorporating GC-MS for product analysis in divided cell is recommended for a better understanding of furfural ECH mechanism at zinc modified electrodes.

APPENDICES

APPENDIX A

BET analysis

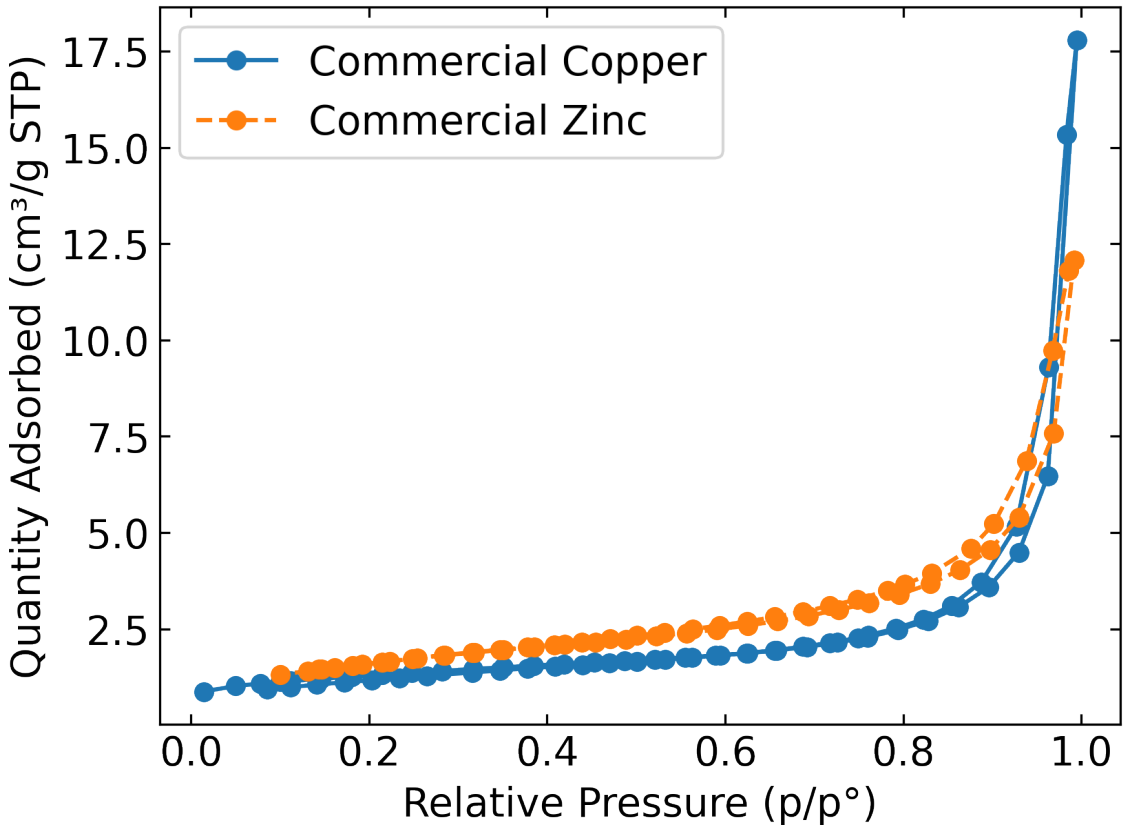

Figure A1. N_2 adsorption-desorption isotherms of commercial zinc and copper nanoparticles.

APPENDIX B

Number of electrons (n) calculation

Number of electrons (*n*) calculation

Number of electrons (*n*) transferred at the electrode surface can be obtained using the following equations:

$$\frac{1}{i} = \frac{1}{i_k} + \frac{1}{i_d} \quad (1)$$

$$i_d = B \cdot n \cdot \omega^{0.5} \quad (2)$$

$$B = 0.62 \cdot F \cdot D^{\frac{2}{3}} \cdot \nu^{-\frac{1}{6}} \cdot C \quad (3)$$

Once Koutecký-Levich plot is generated data can be linearly fitted with a slope of *m*. Using the slope (*m*) of the linearly fitted line, *n* can be calculated.

$$m = \frac{1}{B\,n} = \frac{1}{0.62 \cdot F \cdot D^{\frac{2}{3}} \cdot \nu^{-\frac{1}{6}} \cdot C \cdot n} \quad (4)$$

$$n = \frac{1}{0.62 \cdot F \cdot D^{\frac{2}{3}} \cdot \nu^{-\frac{1}{6}} \cdot C \cdot m} \quad (5)$$

Uncertainty of number of electrons (ω_n) can be solved using the relationship as follows: where $\frac{dn}{dm}$ is a derivate of *n* in terms of *m*, and ω_m is uncertainty of slope.

$$\omega_n = \frac{dn}{dm} \cdot \omega_m \quad (6)$$

$$\frac{dn}{dm} = -\frac{1}{0.62 \cdot F \cdot D^{\frac{2}{3}} \cdot \nu^{-\frac{1}{6}} \cdot C} \cdot \frac{1}{m^2} \quad (7)$$

$$\omega_n = -\frac{\omega_m}{0.62 \cdot F \cdot D^{\frac{2}{3}} \cdot \nu^{-\frac{1}{6}} \cdot C \cdot m^2} \quad (8)$$

BIBLIOGRAPHY

BIBLIOGRAPHY

1. J. Tollefson, "Carbon emissions rapidly rebounded following COVID pandemic dip", *Nature*, (2021). doi:10.1038/d41586-021-03036-x

2. R. L. Ray, V. P. Singh, S. K. Singh, B. S. Acharya and Y. He, "What is the impact of COVID-19 pandemic on global carbon emissions?", *Science of The Total Environment*, **816**, 151503 (2022). doi:10.1016/j.scitotenv.2021.151503

3. BP, *BP Statistical Review of World Energy 2020*, Available at: https:///www.bp.com/en/global/corporate/energy-economics/statistical-review-of-world-energy.html. (accessed April 1, 2022).

4. U.S. Department of Energy, *Biofuel-basics*, Available at: https://www.energy.gov/eere/bioenergy/biofuel-basics. (accessed April 1, 2022).

5. T. Stedile, L. Ender, H. F. Meier, E. L. Simionatto and V. R. Wiggers, "Comparison between physical properties and chemical composition of bio-oils derived from lignocellulose and triglyceride sources", *Renewable and Sustainable Energy Reviews*, **50**, 92–108 (2015). doi:10.1016/j.rser.2015.04.080

6. J. Pérez, J. Muñoz-Dorado, T. de la Rubia and J. Martínez, "Biodegradation and biological treatments of cellulose, hemicellulose and lignin: an overview", *Int Microbiol*, **5**, 53–63 (2002). doi:10.1007/s10123-002-0062-3

7. E. Galiwango, N. S. Abdel Rahman, A. H. Al-Marzouqi, M. M. Abu-Omar and A. A. Khaleel, "Isolation and characterization of cellulose and α-cellulose from date palm biomass waste", *Heliyon*, **5**, e02937 (2019). doi:10.1016/j.heliyon.2019.e02937

8. S. Prasad, A. Singh and H. C. Joshi, "Ethanol as an alternative fuel from agricultural, industrial and urban residues", *Resources, Conservation and Recycling*, **50**, 1–39 (2007). doi:10.1016/j.resconrec.2006.05.007

9. A. Izzotti and A. Pulliero, "The effects of environmental chemical carcinogens on the microRNA machinery", *International Journal of Hygiene and Environmental Health*, **217**, 601–627 (2014). doi:10.1016/j.ijheh.2014.01.001

10. G. Machado, S. Leon, F. Santos, R. Lourega, J. Dullius, M. E. Mollmann and P. Eichler, "Literature Review on Furfural Production from Lignocellulosic Biomass", *NR*, **07**, 115–129 (2016). doi:10.4236/nr.2016.73012

11. D.-R. Hua, Y.-L. Wu, Y.-F. Liu, Y. Chen, M.-D. Yang, X.-N. Lu and J. Li, "Preparation of furfural and reaction kinetics of xylose dehydration to furfural in high-temperature water", *Pet. Sci.*, **13**, 167–172 (2016). doi:10.1007/s12182-015-0069-y

12. K. Yan, G. Wu, T. Lafleur and C. Jarvis, "Production, properties and catalytic hydrogenation of furfural to fuel additives and value-added chemicals", *Renewable and Sustainable Energy Reviews*, **38**, 663–676 (2014). doi:10.1016/j.rser.2014.07.003

13. K. Dalvand, J. Rubin, S. Gunukula, M. Clayton Wheeler and G. Hunt, "Economics of biofuels: Market potential of furfural and its derivatives", *Biomass and Bioenergy*, **115**, 56–63 (2018). doi:10.1016/j.biombioe.2018.04.005

14. Y. P. Wijaya, K. J. Smith, C. S. Kim and E. L. Gyenge, "Electrocatalytic hydrogenation and depolymerization pathways for lignin valorization: toward mild synthesis of chemicals and fuels from biomass", *Green Chem.*, **22**, 7233–7264 (2020). doi:10.1039/D0GC02782K

15. M. Kabbour and R. Luque, "Furfural as a platform chemical", in *Biomass, Biofuels, Biochemicals* (Elsevier, 2020), pp. 283–297. doi:10.1016/B978-0-444-64307-0.00010-X

16. V. R. Koch and J. H. Young, "The Stability of the Secondary Lithium Electrode in Tetrahydrofuran-Based Electrolytes", *J. Electrochem. Soc.*, **125**, 1371–1377 (1978). doi:10.1149/1.2131680

17. S.-H. Jung, B.-S. Kang and J.-S. Kim, "Production of bio-oil from rice straw and bamboo sawdust under various reaction conditions in a fast pyrolysis plant equipped with a fluidized bed and a char separation system", *Journal of Analytical and Applied Pyrolysis*, **82**, 240–247 (2008). doi:10.1016/j.jaap.2008.04.001

18. R. V. Sharma, U. Das, R. Sammynaiken and A. K. Dalai, "Liquid phase chemo-selective catalytic hydrogenation of furfural to furfuryl alcohol", *Applied Catalysis A: General*, **454**, 127–136 (2013). doi:10.1016/j.apcata.2012.12.010

19. X. Shang, Y. Yang and Y. Sun, "Electrohydrodimerization of biomass-derived furfural generates a jet fuel precursor", *Green Chem.*, **22**, 5395–5401 (2020). doi:10.1039/D0GC01720E

20. M. J. Taylor, L. J. Durndell, M. A. Isaacs, C. M. A. Parlett, K. Wilson, A. F. Lee and G. Kyriakou, "Highly selective hydrogenation of furfural over supported Pt nanoparticles under mild conditions", *Applied Catalysis B: Environmental*, **180**, 580–585 (2016). doi:10.1016/j.apcatb.2015.07.006

21. F. Dong, Y. Zhu, G. Ding, J. Cui, X. Li and Y. Li, "One-step Conversion of Furfural into 2-Methyltetrahydrofuran under Mild Conditions", *ChemSusChem*, **8**, 1534–1537 (2015). doi:10.1002/cssc.201500178

22. Z. Li, S. Kelkar, C. H. Lam, K. Luczek, J. E. Jackson, D. J. Miller and C. M. Saffron, "Aqueous electrocatalytic hydrogenation of furfural using a sacrificial anode", *Electrochimica Acta*, **64**, 87–93 (2012). doi:10.1016/j.electacta.2011.12.105

23. D. Chu, Y. Hou, J. He, M. Xu, Y. Wang, S. Wang, J. Wang and L. Zha, "Nano TiO2 film electrode for electrocatalytic reduction of furfural in ionic liquids", *J Nanopart Res*, **11**, 1805–1809 (2009). doi:10.1007/s11051-009-9610-5

24. M. S. Dhawan, G. D. Yadav and S. Calabrese Barton, "Zinc-electrocatalyzed hydrogenation of furfural in near-neutral electrolytes", *Sustainable Energy Fuels*, **5**, 2972–2984 (2021). doi:10.1039/D1SE00221J

25. M. Dhawan, Valorization of Biomass Using Novel Catalytic and Electrocatalytic Processes. Ph.D., Michigan State University, United States -- Michigan, 2021.

26. X. H. Chadderdon, D. J. Chadderdon, J. E. Matthiesen, Y. Qiu, J. M. Carraher, J.-P. Tessonnier and W. Li, "Mechanisms of Furfural Reduction on Metal Electrodes: Distinguishing Pathways for Selective Hydrogenation of Bioderived Oxygenates", *J. Am. Chem. Soc.*, **139**, 14120–14128 (2017). doi:10.1021/jacs.7b06331

27. B. zhao, M. Chen, Q. Guo and Y. Fu, "Electrocatalytic hydrogenation of furfural to furfuryl alcohol using platinum supported on activated carbon fibers", *Electrochimica Acta*, **135**, 139–146 (2014). doi:10/f6b94v

28. Y. Cao and T. Noël, "Efficient Electrocatalytic Reduction of Furfural to Furfuryl Alcohol in a Microchannel Flow Reactor", *Org. Process Res. Dev.*, **23**, 403–408 (2019). doi:10/gfw2n5

29. P. Parpot, A. P. Bettencourt, G. Chamoulaud, K. B. Kokoh and E. M. Belgsir, "Electrochemical investigations of the oxidation–reduction of furfural in aqueous medium", *Electrochimica Acta*, **49**, 397–403 (2004). doi:10/crkgzn

30. W. Xu, C. Yu, J. Chen and Z. Liu, "Electrochemical hydrogenation of biomass-based furfural in aqueous media by Cu catalyst supported on N-doped hierarchically porous carbon", *Applied Catalysis B: Environmental*, **305**, 121062 (2022). doi:10.1016/j.apcatb.2022.121062

31. S. Jung and E. J. Biddinger, "Controlling Competitive Side Reactions in the Electrochemical Upgrading of Furfural to Biofuel", *Energy Technol.*, **6**, 1370–1379 (2018). doi:10.1002/ente.201800216

32. M. Chourashiya, R. Sharma and S. M. Andersen, "Accurate Determination of Catalyst Loading on Glassy Carbon Disk and Its Impact on Thin Film Rotating Disk Electrode for Oxygen Reduction Reaction", *Anal. Chem.*, **90**, 14181–14187 (2018). doi:10.1021/acs.analchem.8b02697

33. X. H. Chadderdon, D. J. Chadderdon, T. Pfennig, B. H. Shanks and W. Li, "Paired electrocatalytic hydrogenation and oxidation of 5-(hydroxymethyl)furfural for efficient production of biomass-derived monomers", *Green Chem.*, **21**, 6210–6219 (2019). doi:10.1039/C9GC02264C

34. J. Suntivich, H. A. Gasteiger, N. Yabuuchi and Y. Shao-Horn, "Electrocatalytic Measurement Methodology of Oxide Catalysts Using a Thin-Film Rotating Disk Electrode", *J. Electrochem. Soc.*, **157**, B1263 (2010). doi:10.1149/1.3456630

35. K. Ke, K. Hiroshima, Y. Kamitaka, T. Hatanaka and Y. Morimoto, "An accurate evaluation for the activity of nano-sized electrocatalysts by a thin-film rotating disk electrode: Oxygen reduction on Pt/C", *Electrochimica Acta*, **72**, 120–128 (2012). doi:10.1016/j.electacta.2012.04.004

36. T. F. Fuller and J. N. Harb, *Electrochemical engineering*, First edition (Wiley, Hoboken, NJ, USA, 2018).

37. S. Wang, K. Uwakwe, L. Yu, J. Ye, Y. Zhu, J. Hu, R. Chen, Z. Zhang, Z. Zhou, J. Li, Z. Xie and D. Deng, "Highly efficient ethylene production via electrocatalytic hydrogenation of acetylene under mild conditions", *Nat Commun*, **12**, 7072 (2021). doi:10.1038/s41467-021-27372-8

38. A. Mainar, L. Colmenares, H.-J. Grande and J. Blázquez, "Enhancing the Cycle Life of a Zinc–Air Battery by Means of Electrolyte Additives and Zinc Surface Protection", *Batteries*, **4**, 46 (2018). doi:10.3390/batteries4030046

39. C. Gumeci, N. Leonard, Y. Liu, S. McKinney, B. Halevi and S. C. Barton, "Effect of pyrolysis pressure on activity of Fe–N–C catalysts for oxygen reduction", *J. Mater. Chem. A*, **3**, 21494–21500 (2015). doi:10.1039/C5TA05995J

40. A. Serov, M. H. Robson, B. Halevi, K. Artyushkova and P. Atanassov, "Highly active and durable templated non-PGM cathode catalysts derived from iron and aminoantipyrine", *Electrochemistry Communications*, **22**, 53–56 (2012). doi:10.1016/j.elecom.2012.04.029

41. P. He, J. Cao, H. Ding, C. Liu, J. Neilson, Z. Li, I. A. Kinloch and B. Derby, "Screen-Printing of a Highly Conductive Graphene Ink for Flexible Printed Electronics", *ACS Appl. Mater. Interfaces*, **11**, 32225–32234 (2019). doi:10.1021/acsami.9b04589

42. M. Lehmann, C. G. Kolb, F. Klinger and M. F. Zaeh, "Preparation, characterization, and monitoring of an aqueous graphite ink for use in binder jetting", *Materials & Design*, **207**, 109871 (2021). doi:10.1016/j.matdes.2021.109871

43. Y. Nadhirah, R. Kusumanto and A. Hasan, "Increasing Efficiency of Dye-Sensitized Solar Cell (DSSC) Originating from Yellow Sweet Potato Extract as Dye Sensitizer: Effect of Acetic Acid, Polyethylene Glycol, and Polyvinyl Alcohol as TiO2 binders", *J. Kim. Sains Apl.*, **23**, 403–408 (2020). doi:10.14710/jksa.23.11.403-408

44. K. C. S. Figueiredo, T. L. M. Alves and C. P. Borges, "Poly(vinyl alcohol) films crosslinked by glutaraldehyde under mild conditions", *J. Appl. Polym. Sci.*, **111**, 3074–3080 (2009). doi:10.1002/app.29263

45. C. M. Pedersen, M. Escudero-Escribano, A. Velázquez-Palenzuela, L. H. Christensen, I. Chorkendorff and I. E. L. Stephens, "Benchmarking Pt-based electrocatalysts for low temperature fuel cell reactions with the rotating disk electrode: oxygen reduction and hydrogen oxidation in the presence of CO (review article)", *Electrochimica Acta*, **179**, 647–657 (2015). doi:10.1016/j.electacta.2015.03.176

46. S. Mohammad Mahdi Dadfar, G. Kavoosi and S. Mohammad Ali Dadfar, "Investigation of mechanical properties, antibacterial features, and water vapor permeability of polyvinyl alcohol thin films reinforced by glutaraldehyde and multiwalled carbon nanotube", *Polym. Compos.*, **35**, 1736–1743 (2014). doi:10.1002/pc.22827

47. J. Masa, C. Batchelor-McAuley, W. Schuhmann and R. G. Compton, "Koutecky-Levich analysis applied to nanoparticle modified rotating disk electrodes: Electrocatalysis or misinterpretation", *Nano Res.*, **7**, 71–78 (2014). doi:10.1007/s12274-013-0372-0

48. K. Yui, N. Yamazaki and T. Funazukuri, "Infinite Dilution Binary Diffusion Coefficients for Compounds Derived from Biomass in Water at 0.1 MPa and Temperatures from (298.2 to 353.2) K", *J. Chem. Eng. Data*, **58**, 183–186 (2013). doi:10.1021/je301060a

49. Biowest, *Safety Data Sheet: Sodium Bicarbonate 7.5% L0680*, Available at: https://www.biowest.net/media/biowest_msds_sodium_bicarbonate_75_l0680.pdf (accessed Feb 26, 2022).

50. S. Lee and S. Calabrese Barton, *Koutecky-Levich-for-ECH*, Available at: https://github.com/scbgroup/Koutecky-Levich-for-ECH

51. S. Azhari, P. Sathishkumar, R. Ahamad, F. Ahmad and A. R. Mohd Yusoff, "Fabrication of a composite modified glassy carbon electrode: a highly selective, sensitive and rapid electrochemical sensor for silver ion detection in river water samples", *Anal. Methods*, **8**, 5712–5721 (2016). doi:10.1039/C6AY01336H

52. Boy. Hoyer, T. Mark. Florence and G. E. Batley, "Application of polymer-coated glassy carbon electrodes in anodic stripping voltammetry", *Anal. Chem.*, **59**, 1608–1614 (1987). doi:10.1021/ac00140a007

53. G. Kefala, A. Economou and A. Voulgaropoulos, "A study of Nafion-coated bismuth-film electrodes for the determination of trace metals by anodic stripping voltammetry", *Analyst*, **129**, 1082 (2004). doi:10.1039/b404978k

54. H. Li, J. Li, Z. Yang, Q. Xu, C. Hou, J. Peng and X. Hu, "Simultaneous determination of ultratrace lead and cadmium by square wave stripping voltammetry with in situ depositing bismuth at Nafion-medical stone doped disposable electrode", *Journal of Hazardous Materials*, **191**, 26–31 (2011). doi:10.1016/j.jhazmat.2011.04.020

55. N. Kumano, K. Kudo, A. Suda, Y. Akimoto, M. Ishii and H. Nakamura, "Controlling cracking formation in fuel cell catalyst layers", *Journal of Power Sources*, **419**, 219–228 (2019). doi:10.1016/j.jpowsour.2019.02.058

56. Pine Research, *E3 Series Rotating Disk Electrode (RDE) Tips*, Available at: https://pineresearch.com/shop/products/electrodes/rde/classic-ptfe/e3/#description (accessed April 9, 2022)

57. M. M. Voigt, R. C. I. Mackenzie, S. P. King, C. P. Yau, P. Atienzar, J. Dane, P. E. Keivanidis, I. Zadrazil, D. D. C. Bradley and J. Nelson, "Gravure printing inverted organic solar cells: The influence of ink properties on film quality and device performance", *Solar Energy Materials and Solar Cells*, **105**, 77–85 (2012). doi:10.1016/j.solmat.2012.04.025

58. J. Sun, X. Ren, Z. Li, W. Tian, Y. Zheng, L. Wang and G. Liang, "Effect of poly (acrylic acid)/Poly (vinyl alcohol) blending binder on electrochemical performance for lithium iron phosphate cathodes", *Journal of Alloys and Compounds*, **783**, 379–386 (2019). doi:10.1016/j.jallcom.2018.12.197

59. N. Rajeswari, S. Selvasekarapandian, C. Sanjeeviraja, J. Kawamura and S. Asath Bahadur, "A study on polymer blend electrolyte based on PVA/PVP with proton salt", *Polym. Bull.*, **71**, 1061–1080 (2014). doi:10.1007/s00289-014-1111-8

60. N. B. R. Kumar, V. Crasta and B. M. Praveen, "Advancement in Microstructural, Optical, and Mechanical Properties of PVA (Mowiol 10-98) Doped by ZnO Nanoparticles", *Physics Research International*, **2014**, 1–9 (2014). doi:10.1155/2014/742378